"Ab-initio" synthesis of zeolites for preestablished catalytic reactions

Eva María Gallego,[+] M. Teresa Portilla,[+] Cecilia Paris, Alejandro León-Escamilla, Mercedes Boronat, Manuel Moliner, Avelino Corma*

Instituto de Tecnología Química, Universitat Politècnica de València-Consejo Superior de Investigaciones Científicas, Avenida de los Naranjos s/n, 46022 Valencia, España

*Corresponding author: E-mail address: acorma@itq.upv.es

[+] These authors have contributed equally

Abstract (100-150 words):

Unlike homogeneous catalysts that are often designed for particular reactions, zeolites are closer to heterogeneous catalysts that are explored and optimized in a heuristic fashion. We present a methodology for synthesizing active and selective zeolites by using organic structure-directing agents that mimic the transition state (TS) of preestablished reactions to be catalyzed. In these zeolites, the pores and cavities could be generated approaching a molecular-recognition pattern. For disproportionation of toluene and isomerization of ethylbenzene into xylenes, the TSs are larger than the reaction products. Zeolite ITQ-27 showed high disproportionation activity, and ITQ-64 showed high selectivity for the desired *para* and *ortho* isomers. For the case of a product and TS of similar size, we synthesized a catalyst, MIT-1, for the isomerization of *endo*-dicyclopentane into adamantane.

One Sentence Summary (150 characters):

The use of OSDAs that mimic reaction transition states allows the synthesis of zeolite catalysts with a better molecular recognition adapted for relevant chemical processes.

Zeolites are used as catalysts for oil conversion, petrochemistry, preparation of chemicals and fine chemicals, as well as for vehicular nitrogen oxide abatements (*1-5*). Although there is a large body of knowledge that helps approach zeolite synthesis and reactivity (*6-11*), trial and error approaches prevail in the synthesis of zeolites and their applicability (testing all known zeolites for a particular reaction is highly labor intensive). "A priori" design and synthesis of a zeolite for catalyzing a pre-established reaction could open new perspectives in the field. A designed catalyst should minimize the free energy ($\Delta G^{\#}$) of the transition state (TS) of the reaction. Tight binding of the catalyst to the TS lowers the activation energy E_a. A zeolite formed in the presence of a particular organic structure-directing agent (OSDA) that is very close in shape and charge to the TS of the reaction to be catalyzed (either new or previously described) should lower E_a.

The methodology described above is connected with the field of "imprinted transition state analogs," where amorphous silica has been used for imprinting mimics of TSs (*12, 13*). However, imprinted amorphous silica has high site heterogeneity, and the "mobility" of the gels upon calcination may disturb the imprinted shapes and terminal groups (*14*). Superior results have been obtained by controlled attachment of functional organic groups to the pores of bulk amorphous silicas (*15, 16*). Then, the imprinting of amorphous oxides method has limitations arising from site accessibility and the lack of stability of the imprinted active voids upon calcination and reaction-regeneration. The advantage with the synthesis of "imprinted" zeolites concept presented here would be the presence of permanent crystalline structures.

We considered two possible scenarios for synthesizing "imprinted zeolites." In the first one, the TS is larger than the reaction product, which allows product could diffuse freely

through the pores of the zeolite. In the second, the product is similar in size to the TS, and product diffusion will be limiting, and could be tested by synthesizing bidimensional zeolites or nanocrystalline zeolites in which the reaction products formed in the discontinued cavities and channels at the external surface could diffuse out.

Toluene disproportionation. The production of xylenes by toluene disproportionation is carried out commercially mainly using ZSM-5 and mordenite catalysts (*17*), where two toluene molecules give one benzene molecule and one dimethylbenzene molecule (*o*-, *m*-, *p*-xylenes). The postulated TS (*18*) is larger than either of the products formed (Fig. 1A). The reported TS molecular structure (*18, 19*) has formal positive charge in the connecting methyl group. An important parameter in selecting between proposed TS mimics (TSMs, see Fig. 1B) is that the location of the positive charge could also fix the position of the active acid site in the structure. In addition to quaternary ammonium groups, the corresponding phosphonium cations were considered as these ions are more stable toward Hoffman degradation than quaternary ammonium ions and allow a wider range of temperature and pH to be explored in synthesis.

We studied the mimics shown in Fig. 1B as OSDAs for the synthesis of zeolites under the reaction conditions presented in the phase diagrams summarized in Fig. S1 in Supplementary Material (SM). Under our synthesis conditions, only one zeolite crystallized when the phosphonium mimic TSM_2 (see Fig. S1 in SM) was used as template. The sample was identified as the previously synthesized ITQ–27 (see PXRD pattern in Fig.S2A in SM) (*20*). The crystalline structure is composed by a bidirectional pore system of interconnected 12x12-ring openings (see Fig. S3 in SM). The zeolite has

been obtained with a Si/Al ratio of 29 (see Table S1 in SM), and crystals are formed as platelets of 1 to 2 μm (see Fig. S4 in SM).

Density Functional Theory (DFT) calculations of the stability of the TSM_2 mimic and of the transition state for toluene disproportionation (TS_TD) inside ITQ-27 zeolite show a very good fitting and energetic stabilization of both cationic species within the ITQ-27 pore system (see computational details and Fig. S5 and Table S3 in SM). These results support the good mimicking effect of the selected OSDA for this target reaction.

We compared the catalytic behavior of the ITQ-27 with the two zeolites industrially used for carrying out disproportionation of toluene, ZSM-5 and mordenite. We selected ZSM-5 and mordenite zeolite samples with the same, or close, Si/Al ratios than ITQ-27 (see experimental details in SM). For comparison, we also introduced a sample of Beta zeolite, where the pore topology (12x12x12-rings) will be closer, but not the same than the ITQ-27 obtained here (12x12-rings), which could also easily accommodate the reaction transition state for the disproportionation reaction. The characterization of the zeolite samples, i.e., crystal size and shape, ^{27}Al MAS NMR and physico-chemical properties are given in Figs. S4 and S6, and Tables S1 and S2 in SM, respectively.

Following a lead from the patent literature on zeolite catalysts for toluene disproportionation (*21, 22*), we have introduced Ni to the zeolites as an hydrogenating function, and then, avoid an excessive catalyst deactivation by coke deposition. The characterization results (see Tables S1 and S2 in SM) indicate that all of the samples considered have a high micropore volume (0.21-0.23 cm^3/g for ITQ-27, Beta_25 and MOR_25, and 0.17 cm^3/g for ZSM-5), and crystallite sites that go from ~1 to 2 μm, except

for the mordenite that presents smaller crystallites (0.2 μm) (see Table S1 in SM). Most of the Al in the zeolite samples are in tetrahedral coordination (see Fig. S6 in SM) and, despite the similar Si/Al ratios, mordenite, and ZSM-5, have a larger amount of Brønsted acid sites than ITQ-27, as measured by pyridine adsorption-desorption (see Table S2 in SM).

The Ni-containing samples were tested for toluene disproportionation in a fixed bed continuous reactor at 450°C and $3 \cdot 10^6$ Pa with a H_2/toluene molar ratio of 4/1. Conversions and selectivities were measured at different contact times (w/F) [catalyst mass (grams) over toluene feed (mol/h)] ranging from 0.1 to 1.1 g. h. mol^{-1} (see experimental in SM). Despite its lower concentration of acid sites, the most active zeolite is ITQ–27 (Fig. 1C). Its activity is very close to mordenite, despite the much larger number of acid sites present in the latter. If the turnover frequencies (TOF) per Brønsted acid site (as measured by pyridine) are calculated from initial reaction rates (Fig. 1D), the order of activity is ITQ-27 > Mordenite ~ Beta > ZSM-5. Moreover, ITQ-27 appears to give the same or even some higher selectivity to xylenes (see Fig. S7 and S8 in SM).

Ethylbenzene isomerization. ZSM-5 and modified ZSM-5 are industrially used to perform the hydroisomerization of xylenes to maximize the *para* isomer. However, the C8 alkylaromatic feed introduced in the process also contains ethylbenzene (EB), which accumulates during the process and should be either dealkylated or isomerized into xylenes. Isomerization is a more carbon-effective process than dealkylation, and zeolite catalysts, and more specifically mordenite, has been used as commercial catalyst for isomerization of EB into xylenes (*23, 24*). The mechanism of EB isomerization may go through a partial ring hydrogenation, followed by protonation-ring-expansion-

deprotonation and ring contraction (see Fig. 2A) (*25*). We mimicked the TS state for EB isomerization into xylenes by preparing a seven-membered ring cationic molecule that could be used as OSDA for zeolite synthesis under different experimental conditions (see Fig. 2B). Results in Fig. S9 in SM show that only amorphous materials were obtained at lower synthesis temperatures (T=135ºC), but at 150 and 175ºC a layered aluminosilicate, named LM1, was obtained along with nonasil, respectively. The powder x-ray diffraction (PXRD) pattern (see Fig. S10 in SM) indicates that LM1 can be a member of the family of layered silicates that form ferrierite (FER) upon calcination, i.e., similar to Prefer (*26*) and PLS-3 (*27*). There are many other layered silicates that feature the pentasil FER-like layers, i.e. ERS-12 (*28*), MCM-47 (*29*), MCM-56 (*30*), PLS-1 and PLS-4 (*27*), UZM-13 (*31*), etc. However, all of them have been shown to transform upon heating into CDO-type zeolite. Thus, this latter subfamily of layered silicates should more properly be referred as precursors of CDO, or pre-CDO materials.

The PXRD patterns of LM1 and LM1 after calcination (CLM1) resemble those of Prefer and FER materials (see Fig. S10 in SM). The PXRD patterns of LM1 and CLM1 have been indexed for orthorhombic cells with cell dimensions: a=13.992(3) Å, b=7.455(2) Å, and c= 22.847(8) Å and, a=14.106(1) Å, b=7.4530(5) Å, and c= 18.780(1) Å, respectively (see Table S4 in SM). Taking the FER structure as reference (see CLM1 in Table S4 in SM), there is a 4.07 Å increment in the c axis in LM1 that implies ~2.03 Å between pentasil layers. The structure of LM1 is likely held together by hydrogen-bond interactions of silanols from neighboring layers, $\equiv Si_L–O(H)::(H)O–Si_L\equiv$ (Si_L refers to silicon atoms in the pentasil layers, see Fig. S11 in SM). Comparison of the ^{13}C cross-polarization magic-angle spinning nuclear magnetic resonance spectroscopy (CPMAS-NMR) spectrum of the as-prepared LM1 and the ^{13}C-NMR of the OSDA indicates that

the trapped organic molecule was stable during the synthesis (see Fig. S12 in SM). DFT calculations reveal a very good geometrical adjustment of the TSM_4 mimic within the channels of the LM1 material, presenting a large interaction energy value of -190.6 kcal mol^{-1} (see Fig. S13 and Table S3 in SM).

For catalytic applications, the final pore of the zeolite must remain almost the same as that of the expanded pore of the LM1 synthesized with the OSDA. Thus, we could not simply heat the sample to produce the zeolite because the pore would contract and not be able to accommodate the TS of the reaction. Instead, we performed "self-pillaring" with an acid treatment of LM1 [(*32*), see also experimental details in SM] that introduced one Si to bridge the layers (see Fig. S11 in SM). This zeolite structure, named ITQ-64, has a pore topology formed by 12x10 rings (see Fig. S11 in SM). An analysis of the PXRD pattern of ITQ-64 indicates that it should be a more ordered variation of APZ-4 (*32*) and one variation of IEZ-FER (*33*). If the structure of ITQ-64 is nearly the same as that of APZ-4, we can calculate cell dimensions of *a*= 14.032(1) Å, *b*= 7.4120(6) and *c*=23.744(2) Å (see Table S4 in SM). With respect to LM1, the cell of ITQ-64 is 0.9 Å longer on the *c* axis, normal to the stacking plane. Such an expansion refers to the substitution at z=0 and ½ of the contact $\equiv Si_L–O(H)::(H)O–Si_L\equiv$ in LM1 for the new linkage unit ($\equiv Si_L–O–Si(OH)_2–Si_L$) in ITQ-64. The micropore volume of ITQ-64 is 0.14 $cc.g^{-1}$ (see Table S5 in SM), and crystals are formed as platelets of 1 to 2 μm (see Fig. S14 in SM). The ITQ-64 material has a Si/Al ratio near 50 (see Table S5), indicating that the Si/Al ratio remained fairly constant after the pillaring acid treatment and, very interestingly, these Al species were retained in the zeolite framework (see ^{27}Al MAS NMR spectrum of ITQ-64 in Fig. S15A in SM).

The interaction of the transition state for EB isomerization (TS_EI) with the ITQ-64 material was also studied using DFT calculations and a high interaction energy value of -182.4 kcal mol^{-1} was obtained, in line with the excellent molecular confinement of the cationic transition state inside ITQ-64 structure (see Fig. S13 and Table S3 in SM).

A commercial catalyst for EB isomerization (a bifunctional Pt/mordenite catalyst) can catalyze the different reaction steps shown in Fig. 2A *(24)*. Indeed, the hydrogenating metal function will partially hydrogenate the aromatic ring, which after protonation on the acid sites will form the expanded C7 protonated ring *(34)*. We compared ITQ-64 with two mordenite catalysts containing different Si/Al molar ratios (22 and 47, see MOR_25 and MOR_47, respectively in Table S5 in SM), after combining all of these zeolites with 1%wt Pt/Al_2O_3 to introduce the required hydrogenating function (see catalyst preparation in SM).

When testing these zeolites at the same contact time (~ 5 g.h/mol), the high-silica mordenites had higher ethylbenzene conversion values compared to ITQ-64 (see Table 1). The higher Brønsted acidities of the mordenite materials, as measured by pyridine (see Table S6 in SM), could explain their higher catalytic activities, but if the turnover frequencies (TOF) per Brønsted acid site are calculated from initial reaction rates, ITQ-64 showed the highest catalytic activity (see Fig. S16 in SM). Morover, ITQ-64 showed higher xylene selectivities compared to the mordenites (see Table 1), even when the zeolites are compared at similar level of conversion (~30%, see Table 1), and ITQ-64 showed higher aromatic selectivity to xylenes than the reported mordenites (see Fig. S17 in SM). The most desired isomers are *p*-xylene, a precursor of polyester (more than 60% of total xylene consumption), and the *o*-xylene, used to produce polyester and plasticizers

(around 14% of total xylene consumption). The ITQ-64 material provides higher overall selectivity towards *p*- and *o*-xylenes than the high-silica mordenite zeolites, substantially diminishing the selectivity toward the less desired *m*-xylene (see Figs. 2C and 2D, and Table S7 in SM).

Adamantane synthesis. Adamantane and its derivatives are important tricyclic saturated hydrocarbons for the fields of pharmaceuticals and polymers *(35)*. The most efficient route to prepare adamantane at an industrial scale is from *endo*-dicyclopentadiene (see Fig. S18 in SM) *(36-38)* via hydrogenation and then using aluminum chloride to catalyze the isomerization from the endo to exo isomer and then to adamantane (see Fig. 3A). To avoid the environmental problems associated with aluminum chloride, environmentally friendly solid-acid isomerization catalysts would be preferable. Zeolite Y has been the leading catalyst of the few actually studied *(39-41)*.

Mechanistic studies of the adamantane synthesis have proposed that the second isomerization to adamantane is rate controlling and occurs through carbocationic species (Fig. 3A) (*42*). The intermediate of the rearrangement reaction presents a similar conformation, including shape and size, to the adamantane product (Fig. 3A), so a cavity to accommodate the intermediate could be made via an OSDA with the adamantane structure, such as *N*,*N*,*N*-trimethyladamantammonium (TSM_5, Fig. 3B), a molecule that has been used extensively as an OSDA for the silicoaluminate SSZ-13 zeolite (CHA structure) (*43*). This zeolite is a cage-based material delimited by small pores (3.5 Å) that will not allow the diffusion of the reactants and products involved in the reaction. TSM_5 has also been used to synthesize ITQ-1, the high-silica form of the MWW material *(44)*.

Unfortunately, the use of the TSM_5, as the only OSDA, preferentially directs the crystallization of the pure silica ITQ-1 material, precluding its application as acid catalyst.

The crystalline structure of the MWW material is formed by two independent channels with 10-ring pore openings (~5.5 Å), and containing a supercage of 7.1×7.1×18.2 Å (see Fig. S19a in SM). This supercage, which is stabilized by the TSM_5 molecule, allows envisioning that the cage-based MWW-type material would permit maximizing the host-guest interactions with the TS of the adamantane isomerization reaction. However, the presence of the medium pores would present severe diffusion restrictions. Nonetheless, the cage accessibility may be remarkably improved by preparing the zeolite in 2D form (see Fig. S19b in SM) to reduce diffusion limitations of the reactant and products.(*45*)

The direct synthesis of the 2D form of the MWW was achieved recently by using bifunctional OSDAs with a cationic head that allows the crystallization of the MWW layers, and a long aliphatic chain that avoid the layers to grow and order along the *c* axis *(46, 47)*. More specifically, this MIT-1 material was synthesized with an OSDA containing TSM_5 as the cationic head, which can be considered as the TS mimic of the tricyclodecane isomerization (see TSM_6 in Fig. 5B). The PXRD pattern of the corresponding 3D MCM-22 (a MWW material) shows better crystallinity than that of the MIT-1 material (see Fig. S20 in SM), as it could be expected by its larger order along the *c* axis (see Fig. S19a in SM). Thus, MIT-1 presents larger external surface area formed by "open" cups versus MCM-22 (see Table S8 in SM). The acid properties of these materials is shown in Table S9.

Two large pore zeolites, Beta and USY, were tested for catalytic activity. Despite high *endo*-tricyclodecane conversions, but their selectivity toward adamantane was very low

for both materials (~5 and 11%, respectively, see Table 2). Their high catalytic activity could be attributed to the presence of large pores in these materials, providing better diffusion pathways to the decane isomers, in line with previous reports (*41*) (see Table 2). In contrast, the two MWW-related materials show a remarkable increase in the selectivity toward the desired adamantane product (above 30%), which is higher than the selectivity observed for the other commercial zeolites (below 11%, see Table 2). This observation could be explained by the adequate fit between the TS of the tricyclodecane isomerization reaction within the MWW-cavity. Indeed, the MIT-1 catalyst, synthesized with a bifunctional TSM of the tricyclodecane isomerization reaction with the aim of favoring not only the formation of MWW cavities but also their accessibility, shows a substantial increase of the catalytic activity compared to MCM-22 while maintaining the high adamantane selectivity (~33%, see Table 2). Other MWW-related materials, such as the partially-condensed MCM-56 material and the highly-delaminated ITQ-2 material, have also been tested to further support the concept. As seen in Table 2, MCM-56 shows comparable results to those achieved with MCM-22, while ITQ-2 results resemble more those of MIT-1.

The zeolite synthesis methodology based on the design of TS mimics of relevant industrial reactions to be used as OSDAs for the synthesis of target zeolites, has allowed improving the catalytic activity and selectivity of different chemical and petrochemical processes compared to other commercial zeolitic catalysts. In general, the concept presented here can provide new opportunities for designing more selective adsorption and catalytic solids, as well as sensors and molecular responsive solids.

References:

1. W. Vermeiren, J. P. Gilson, *Top. Catal.* **52**, 1131-1161 (2009).
2. M. J. Climent, A. Corma, S. Iborra, *Chem. Rev.* **111**, 1072-1133 (2011).
3. D. E. De Vos, P. A. Jacobs, *Micropor. Mesopor. Mater.* **82**, 293-304 (2005).
4. P. A. Jacobs, M. Dusselier, B. F. Sels, *Angew. Chem., Int. Ed.* **53**, 8621-8626 (2014).
5. P. Y. Dapsens, C. Mondelli, J. Perez-Ramirez, *ACS Catal.* **2**, 1487-1499 (2012).
6. M. E. Davis, *Chem. Mater.* **26**, 239-245 (2014).
7. M. Moliner, F. Rey, A. Corma, *Angew. Chem., Int. Ed.* **52**, 13880-13889 (2013).
8. J. E. Schmidt, M. W. Deem, M. E. Davis, *Angew. Chem., Int. Ed.* **53**, 8372-8374 (2014).
9. P. Eliasova *et al.*, *Chem Soc. Rev.* **44**, 7177-7206 (2015).
10. A. Bhan, A. D. Allian, G. J. Sunley, D. J. Law, E. Iglesia, *J. Am. Chem. Soc.* **129**, 4919-4924 (2007).
11. M. Boronat, C. Martínez-Sánchez, D. Law, A. Corma, *J. Am. Chem. Soc.* **130**, 16316-16323 (2008).
12. J. Heilmann, W. F. Maier, *Angew. Chem., Int. Ed.* **33**, 471-473 (1994).
13. G. Wulff, B. Heide, G. Helfmeier, *J. Am. Chem. Soc.* **108**, 1089-1091 (1986).
14. W. R. Ahmad, M. E. Davis, *Catal. Lett.* **40**, 109-114 (1996).
15. A. Katz, M. E. Davis, *Nature* **403**, 286-289 (2000).
16. J. E. Lofgreen, G. A. Ozin, *Chem. Soc. Rev.* **43**, 911-933 (2014).
17. T. C. Tsai, S. B. Liu, I. Wang, *Appl. Catal. A* **181**, 355-398 (1999).
18. J. Cejka, B. Wichterlova, *Catal. Rev.* **44**, 375-421 (2002).
19. Y. Xiong, P. G. Rodewald, C. D. Chang, *J. Am. Chem. Soc.* **117**, 9427-9431 (1995).
20. D. L. Dorset *et al.*, *J. Am. Chem. Soc.* **128**, 8862–8867 (2006).
21. X. Xiao, J. Butler, C. Comeaux, K. K., *U.S. Patent 20060211902, 2006*.
22. J. R. Butler, X. Xiao, R. Hall, *U.S. Patent 20080319243, 2008*.
23. F. Moreau *et al.*, *J. Catal.* **202**, 402-412 (2001).
24. L. D. Fernandes, J. L. F. Monteiro, E. F. Sousa-Aguiar, A. Martinez, A. Corma, *J. Catal.* **177**, 366-377 (1998).
25. H. Pines, T. W. Greenlee, *J. Org. Chem.* **26**, 1052-1057 (1961).
26. L. Schreyeck, P. Caullet, J. C. Mougenel, J. L. Guth, B. Marler, *Micropor. Mater.* **6**, 259-271 (1996).
27. T. Ikeda, S. Kayamori, F. Mizukami, *J. Mater. Chem.* **19**, 5518-5525 (2009).
28. R. Millini *et al.*, *Microporous Mesoporous Mater.* **74**, 59-71 (2004).
29. A. Burton, R. J. Accardi, R. F. Lobo, M. Falconi, M. W. Deem, *Chem. Mater.* **12**, 2936-2942 (2000).
30. D. L. Dorset, G. J. Kennedy, *J. Phys. Chem. B* **108**, 15216-15222 (2004).
31. L. M. Knight *et al.*, *Stud. Surf. Sci. Catal.* **170**, 338-340 (2007).
32. T. Ikeda, S. Kayamori, Y. Oumi, F. Mizukami, *J. Phys. Chem. C* **114**, 3466-3476 (2010).
33. J. Ruan *et al.*, *Chem. Mater.* **21**, 2904–2911 (2009).
34. K. H. Robschlager, E. G. Chrlstoffe, *Ind. Eng. Chem. Prod. Res. Dev.* **18**, 347-352 (1979).
35. *Advances in adamantane research and application, Ed. Q. A. Acton, ScholarlyEditions, Atlanta, 2013*.
36. P. R. Schleyer, *J. Am. Chem. Soc.* **79**, 3292–3292 (1957).
37. E. M. Engler, M. Farcasiu, A. Sevin, J. M. Cense, P. V. R. Schleyer, *J. Am. Chem. Soc.* **95**, 5769-5771 (1973).
38. G. C. Lau, W. F. Maier, *Langmuir* **3**, 164-173 (1987).
39. K. Honna, M. Sugimoto, N. Shimizu, K. Kurisaki, *Chem. Lett.*, 315-318 (1986).
40. Z. Gao, H. B. Yang, *Chin. J. Chem.* **12**, 52-57 (1994).
41. M. Navrátilová, K. Sporka, *Appl. Catal. A* **203**, 127-132 (2000).
42. P. R. Schleyer, M. M. Donaldson, *J. Am. Chem. Soc.* **82**, 4645-4651 (1960).

43. S. I. Zones, *U.S. Patent 4544538, 1985*.
44. M. J. Diaz, M. A. Camblor, C. Corell, A. Corma, *US Patent, 6077498, 2000*.
45. A. Corma, V. Fornes, S. B. Pergher, T. L. M. Maesen, J. G. Buglass, *Nature* **396**, 353-356 (1998).
46. H. Y. Luo, V. K. Michaelis, S. Hodges, R. G. Griffin, Y. Roman-Leshkov, *Chem. Sci.* **6**, 6320-6324 (2015).
47. V. J. Margarit, M. E. Martínez-Armero, M. T. Navarro, C. Martínez, A. Corma, *Angew. Chem., Int. Ed.* **54**, 13724 -13728 (2015).
48. E. Mishani *et al.*, *US2011/0293519, 2011*.
49. D. Marcoux, A. B. Charette, *J. Org. Chem.* **73**, 590-593 (2008).
50. M. K. Rubin, P. Chu, *U.S. Patent 4954325, 1990*.
51. A. S. Fung, S. L. Lawton, W. J. Roth, *U.S. Patent 5362697, 1994*.
52. C. A. Emeis, *J. Catal.* **141**, 347-354 (1993).
53. J. P. Perdew *et al.*, *Phys. Rev. B* **46**, 6671-6687 (1992).
54. J. P. Perdew, Y. Wang, *Phys. Rev. B* **45**, 13244-13249 (1992).
55. G. Kresse, J. Furthmüller, *Phys. Rev. B* **54**, 11169-11186 (1996).
56. P. E. Blöchl, *Phys. Rev. B* **50**, 17953-17979 (1994).
57. S. Grimme, J. Antony, S. Ehrlich, H. Krieg, *J. Chem. Phys.* **132**, 154104 (2010).
58. V. V. Narkhede, H. Gies, *Chem. Mater.* **21**, 4339-4346 (2009).

ACKNOWLEDGMENTS

This work has been supported by the European Union through ERC-AdG-2014-671093 (SynCatMatch), and the Spanish Government through "Severo Ochoa Program" (SEV 2012-0267). The Electron Microscopy Service of the UPV is acknowledged for their help in sample characterization. The Red Española de Supercomputación (RES) and Centre de Càlcul de la Universitat de València are gratefully acknowledged for computational facilities and technical assistance. E.M.G. acknowledges "La Caixa - Severo Ochoa" International PhD Fellowships (call 2015). We thank I. Millet for technical assistance, and V. J. Margarit and Á. Cantín for helpful discussions.

SUPPLEMENTARY MATERIALS

www.sciencemag.org/content/XXXXX

Materials and Methods

Figs. S1 to S20

Tables S1 to S9

References (*48-58*)

Fig. 1. Toluene disproportionation. (A) Reaction mechanism for the acid catalyzed toluene disproportionation reaction. (B) Proposed toluene transalkylation transition state mimics (TSM) as organic structure directing agents (OSDAs). (C) Toluene conversion obtained for the toluene disproportionation reaction in vapor phase at 450°C and $3 \cdot 10^6$ Pa with 30 s of time-on-stream (TOS) under different contact times (w/F = 0.1-1.1 g.h/mol). (D) TOF normalized per measured acid site (B150) at different WHSV

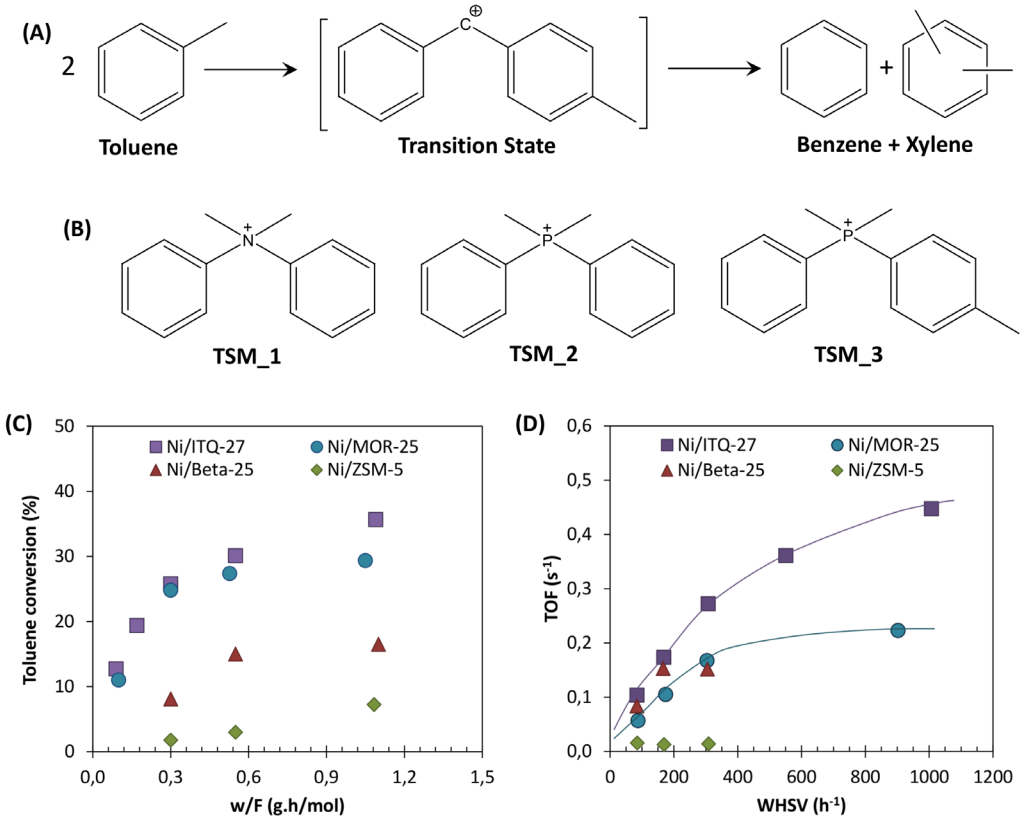

Fig. 2. Ethylbenzene (EB) isomerization. (A) Reaction mechanism for the acid catalyzed EB isomerization reaction toward xylenes. (B) Proposed EB isomerization transition state mimic (TSM) as organic structure directing agent (OSDA). (C and D) Selectivity to xylene isomers versus time-on-stream (TOS) for the EB isomerization reaction using different zeolites

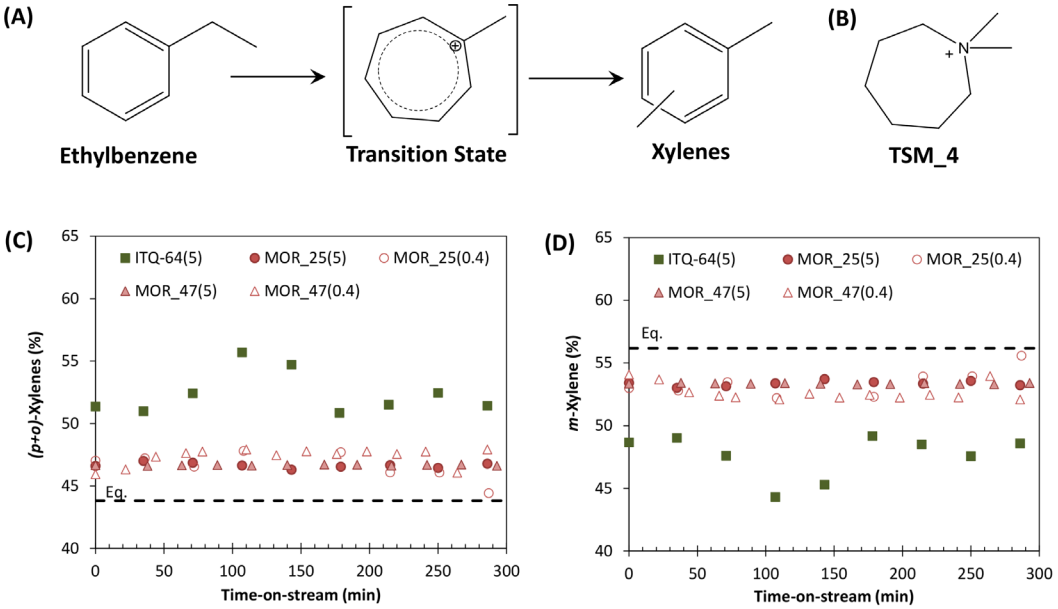

Fig. 3. Adamantane synthesis. (A) Reaction mechanism for the *endo*-tricyclodecane isomerization. (B) Proposed OSDAs as TSM for the *endo*-tricyclodecane isomerization

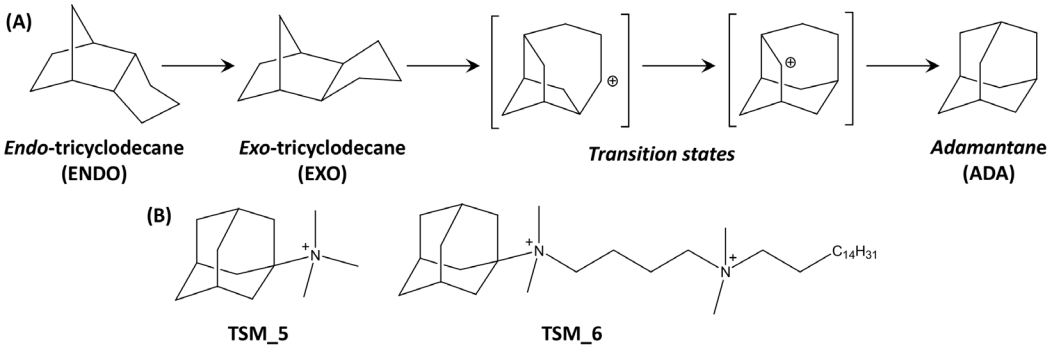

Table 1. Ethylbenzene conversion and product distribution achieved for the ethylbenzene isomerization using different zeolites (TOS = 30 min)

Catalyst	**ITQ-64**	**MOR_25 (Si/Al=22)**		**MOR_47 (Si/Al=47)**	
m_{cat} (g)	1.00	0.15	1.00	0.13	1.00
w/F (g·h/mol)	5.06	0.38	5.06	0.40	5.06
EB conversion (%)	26.4	33.4	79.6	25.4	71.1
Yield (wt.%)					
Light HC	14.0	14.2	37.6	7.4	30.0
Aromatic HC	12.4	19.2	42.0	18.0	41.0
Aromatic Select. (wt.%)					
Benzene	11.0	31.7	39.4	33.1	38.5
Toluene	2.8	4.3	19.7	2.4	15.1
Xylenes	63.3	28.6	17.4	19.9	17.2
Diethylbenzenes	9.1	25.4	6.9	38.4	14.1
Trimethylbenzenes	0.3	2.4	2.1	0.5	1.6
Other aromatics	6.4	5.9	11.2	4.5	10.3
C10+ aromatics	7.2	1.6	3.2	1.2	3.2

Table 2. Catalytic activity for the *endo*-tricyclodecane isomerization at 300°C and 6.10^6 Pa

Catalyst	Time (min)	TMN conversion (%)	Selectivity EXO (%)	Selectivity ADA (%)
USY (CBV-720)	75	55.0	32.4	11.2
	180	72.0	29.6	11.4
Beta (CP811)	180	56.9	14.8	4.6
MCM-22	180	37.8	13.3	30.2
MCM-56	180	28.7	14.9	24.1
ITQ-2	180	54.0	14.2	31.8
MIT-1	180	50.8	16.8	33.4